JJEE
Volume 6, Number 4, 2020
Pages 334-346
Jordan Journal of Electrical Engineering
ISSN (Print): 2409-9600, ISSN (Online): 2409-9619

Influence of Oblique Incidence on the Reflection Losses in a Multilayer Human Body Medium

Rula Alrawashdeh*

Electrical Engineering Department, College of Engineering, Mutah University, Mutah, Jordan
E-mail: rularsr18@gmail.com

Received: May 10, 2020 *Revised: June 25, 2020* *Accepted: June 30, 2020*

***Abstract*—** Implantable antennas have many important healthcare applications. One key aspect for a successful communication process from the implantable device to the on or off-body receiver is the accurate evaluation of the in-body path losses. These losses include, mainly, the attenuation and the reflection losses. Usually, normal incidence is considered for the calculation of the reflection losses between the tissue layers. However, this is not very accurate as the incident wave may be oblique at the boundary between the tissue layers. Therefore, in this paper the influence of oblique incidence on the reflection losses in a multilayer human body model is investigated. The reflection losses at the bone/muscle, muscle/fat and fat/skin layers are calculated at 403 MHz considering the cases of parallel and perpendicular polarization oblique incidence. The results are analyzed and compared with those of normal incidence. They show that larger losses are obtained at some angles for the case of oblique incidence compared to those for the case of normal incidence (about 241.16% larger reflection loss is obtained at an incident angle of 85° for the case of oblique incidence/perpendicular polarization at the fat/skin interface in comparison with that for normal incidence). Hence, it is very important to take the oblique incidence into consideration to provide more accurate in-body path loss calculations.

***Keywords*—** Normal incidence; Oblique incidence; Parallel polarization; Perpendicular polarization; Reflection coefficient; Reflection losses.

1. INTRODUCTION

Implantable devices have a vital role in healthcare applications such as glucose monitoring [1-3]. The implant is composed of different components that sense, process and send the bio-signals to body worn or external receivers around the human body [4-6]. The location of the implantable device – whether it is in the bone, deep in the muscle or just beneath the skin - is mainly influenced by the application [7]. The signals transmitted from the implantable device pass through different human body tissues till they reach the receiver. During this process, the signals are susceptible to absorption and reflection losses. The power absorption is mainly caused by attenuations in the lossy tissue layers while reflection losses are attributed to the difference in the dielectric properties between tissue layers [8]. The path loss is an important parameter in estimating the communication range or specifying the required implantable transceiver characteristics such as the required input power or receiver sensitivity [9]. Hence, these losses should be estimated accurately to provide accurate link budget calculations for the intended application. However, this is not an easy task for a complicated channel such as the human body, which is composed of multiple layers [10]. The path losses were either calculated in heterogeneous and non-uniform anatomical body models or in uniform multilayer tissues. In [11], the in-to-out body path loss was estimated and modeled for multilayered and heterogeneous medium at 2.4 GHz. That path loss estimation was specified for a commercial anatomical body model provided by SEMCAD-X

* Corresponding author
Article's DOI: 10.5455/jjee.204-1589141623

software tool. In [12], the path loss between muscle and bone implants was estimated at 403 MHz. However, the estimation was also for a specific anatomical model provided by the CST software package. Another model of the path loss in the anatomical model was suggested and discussed in [13] between an endoscopy capsule and a receiver outside the human body. It is obvious that the results obtained in [11-13] were for specific body models and they will be different for other anatomical body models. Hence, these results cannot be generalized. This issue was confirmed in [14] where the path loss was computed in the gastrointestinal tract of different anatomical body models provided by SEMCAD-X at 2.4 GHz. The study showed that in 50% of the cases - at the same capsule location in any of the models - the obtained losses were different. This was due to the fact that different human subjects are significantly different in terms of the body mass and size. To overcome the issue of estimating the path loss for each model in specific, the path loss can be calculated in a uniform body model that resembles the structure of the human body and then extra losses can be added as a link margin [9, 15, 16]. The value of the link margin can then substitute the effect of the human body structure and gender. This concept was followed in [17] where the path loss was calculated and analyzed in a simplified human body model of a uniform multilayer structure. The path loss was analyzed in [18] in a multilayer digestive tract model. However, the analysis considered mainly the attenuation losses while the reflection losses were not investigated. In [19], the path loss was only calculated in a single muscle layer. The overall path loss in a simplified multilayer body model of the human leg was calculated in [20] taking into consideration both the attenuation and the reflection losses. Although the path losses in [17] and [20] included the reflection losses in addition to the attenuation losses, they were calculated assuming the case of normal incidence only. However, oblique incidence is possible and thus should be analyzed [21]. Larger losses than that of normal incidence is possible at some angles. This means that the overall path losses may be underestimated if this case of oblique incidence is not taken into account. Therefore, this paper is focused to investigate the effect of oblique incidence on the reflection losses in a multilayer human body model. The results in this paper are important to provide an accurate estimation of the in-body path losses and hence, to provide accurate link budget calculations. Up to the author's best knowledge, the investigations on the influence of oblique incidence on the reflection and in-body path losses proposed in this paper, are new and have not been reported in literature.

This paper is arranged as follows: in section 2, the parameters and characteristics of the channel model is provided. In section 3, the reflection losses due to normal and oblique incidence are calculated and compared. The relationship between the angles of incidence and reflection losses are analyzed for both of parallel and oblique incidence in section 4. The paper is finally concluded in section 5.

2. THE CHANNEL MODEL

The human body is composed of multiple tissue layers of different thicknesses. Implants are usually placed inside either bone or muscle. The implants in the muscle are either placed deep inside it, or just beneath the skin. The wave usually passes through bones, muscles, fat and skin to the air. The wave is susceptible to attenuation losses in the tissue layer and to reflection losses at the boundaries between tissues. This paper aims at

calculating the reflection losses between the human body tissues. The propagation channel in this paper is modeled as multiple layers composed of: bone, muscle, fat, and skin. This model is shown in Fig. 1. A rectangular shape is selected to simplify the analysis while obtaining reliable calculation results at the same time. This model resembles the multilayer structure of real human body. It can be considered reliable enough for the intended calculations as reflection losses are usually calculated considering a plane boundary between the human body tissue layers which is always the case even if different model shapes (circular or rectangular) are considered.

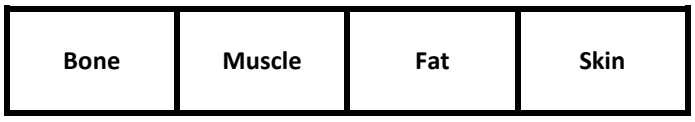

Fig. 1. Model of the investigated channel.

Human body tissues are heterogeneous and their dielectric properties are frequency dependent. The 401-406 MHz Medical Device Radio communications band has been allocated for data transmission of implantable applications [22, 23]. The selection of this band has the following advantages for in-body communication:

- Relatively small losses are obtained in this band, especially if compared with losses at higher frequencies in the GHz range, because the conductivity of human body tissues and attenuation losses increase with frequency.
- Limitations of inductive links used for in-body communication (i.e. short communication range, issues of misalignment between the coils, low data rates and slow transmission) are overcame [24].

Hence communication in this band provides an optimum choice for in-body communications as it enables reasonable data rates, relatively small losses and longer communication ranges than inductive links. The 403 MHz which is the center frequency of this band has been selected for the calculations in this paper.

3. CALCULATIONS AND ANALYSIS

In this section, the reflection losses at the boundary between each two layers of the model are calculated. The reflection losses L_r[dB] are calculated as [20, 25]:

$$L_r = 20log_{10}(|\Gamma|) \quad (1)$$

where |Γ| is the reflection coefficient magnitude. The value of the reflection coefficient differs for the cases of normal and oblique incidence. In normal incidence, the incident wave is normal to the boundary between the media. In oblique incidence, the incident wave is oblique at the boundary making some angles with it. Two cases for oblique incidence are assumed depending on whether the wave fields are in the plane of incidence or perpendicular to it. In this section, the reflection losses are calculated for three cases, namely normal incidence, parallel polarization oblique incidence and perpendicular polarization oblique incidence.

3.1. Normal Incidence

As indicated above, the incident wave is normal to the boundary between the media for this case. Normal incidence is illustrated in Fig. 2. It can be seen from the figure that two regions below and above z= 0 exist around the boundary. The incident wave is propagating from the first region or medium (z< 0) to the second region or medium (z> 0) in a direction normal to the interface (the direction of propagation is indicated by the unit vector ($\vec{a}_k$) which is $\vec{a}_z$ for this case). The electric ($\vec{E}$) and magnetic ($\vec{H}$) fields of which the wave is composed are in a plane normal to the axis of propagation (the xy-plane in this case).

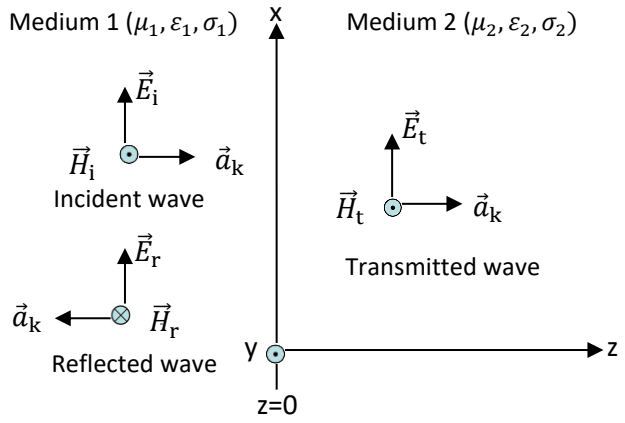

Fig. 2. Normal incidence [8]; $\vec{E}_i$, $\vec{E}_r$ and $\vec{E}_t$ are the incident, reflected and transmitted electric field intensities, respectively; $\vec{H}_i$, $\vec{H}_r$ and $\vec{H}_t$ are the incident, reflected and transmitted magnetic field intensities, respectively.

For the body model exhibited in Fig. 1, the media represent the human body tissues while the boundary is the interface between these tissues. The proportion of the incident wave that is reflected or transmitted depends on the constitutive parameters (μ, ε, σ) of the two tissues involved:

$$\Gamma = \frac{\eta_2 - \eta_1}{\eta_2 + \eta_1} \tag{2}$$

where Γ is the reflection coefficient, η_1 and η_2 [Ω] are the intrinsic impedances of the first and second tissue layers between which the reflection coefficient is calculated. The intrinsic impedance η [Ω] of the tissue layer is defined as:

$$\eta = \sqrt{\frac{j\omega\mu}{\sigma + j\omega\varepsilon}} \tag{3}$$

where μ [H/m] is the magnetic permeability which is equal to μ_0 for the nonmagnetic human body tissues, σ [S/m] is the electric conductivity and ω [rad/m] is the radian frequency, and ε [F/m] is the electric permittivity which is calculated as:

$$\varepsilon = \varepsilon_0 \varepsilon_r \tag{4}$$

where ε_0 is the free space permittivity given as 8.854E-12 F/m and ε_r is the relative permittivity (dielectric constant) which is unitless.

In lossy media such as the human body tissues, the intrinsic impedance is a complex quantity that is represented by a magnitude |η| and phase θ_η which can be calculated as [8]:

$$\eta = |\eta| \angle \theta_\eta \quad (5)$$

$$|\eta| = \frac{\sqrt{\mu/\varepsilon}}{\left(1 + (\frac{\sigma}{\omega\varepsilon})^2\right)^{1/4}} \quad (6)$$

$$\tan 2\theta_\eta = \frac{\sigma}{\omega\varepsilon} \quad (7)$$

where the factor $(\frac{\sigma}{\omega\varepsilon})$ is the loss tangent which is an important parameter in defining the behavior of lossy media at different frequencies.

The dielectric properties of bone, muscle, fat and skin at 403 MHz are summarized in Table 1 [26].

Table 1. Dielectric properties of bone, muscle, fat and skin at 403 MHz [26].

The tissue layer	ε [F/m]	σ [S/m]	Loss tangent
Bone	13.14	0.092	0.31
Muscle	57.1	0.797	0.62
Fat	5.58	0.041	0.33
Skin	46.72	0.69	0.66

The intrinsic impedance for each tissue layer of investigation is calculated based on the parameters in Table 1 and its values are summarized in Table 2.

Table 2. The intrinsic impedance η of the model layers at 403 MHz.

The tissue layer	η [Ω]	
	Polar form	Rectangular form
Bone	$101.6 \angle 8.6^o$	100.5+j15.2
Muscle	$45.96 \angle 15.9^o$	44.2+j12.59
Fat	$155.41 \angle 9.1^o$	153.45+j24.58
Skin	$50.35 \angle 16.7^o$	48.23+j14.47

The largest intrinsic impedance is obtained for fat which has the smallest value of permittivity amongst the investigated tissues.

The total reflection losses in such a case can be calculated using Eq. (1). The wave is assumed to transfer from bone to muscle, muscle to fat and fat to skin which is the boundary between the human body and free space. The results are summarized in Table 3.

Table 3. The reflection coefficient Γ and reflection loss at 403 MHz between the tissue layers.

The interface	Γ $\lvert\Gamma\rvert \angle \theta_\Gamma{}^o$	The reflection loss [dB]
Bone/muscle	$0.38 \angle 171.51$	-8.4
Muscle/fat	$0.55 \angle -4.3$	-5.19
Fat/skin	$0.51 \angle 174.53$	-5.85

Eq. (1) indicates that the reflection losses are mainly influenced by the reflection coefficient magnitude which increases if the difference in the intrinsic impedances and relative permittivity between the body tissues is increased. Hence, the largest reflection

coefficient and loss (less negative) are obtained at the muscle/fat boundary which have the largest difference in the relative permittivity values between the muscle and the fat tissues. Followed by the reflection loss for the fat/skin boundary for which the fat and skin tissues have also a large difference in their permittivity values but this difference is smaller than that for the muscle/fat boundary. The smallest reflection loss (most negative) is obtained for the bone/muscle interface as the difference in the permittivity values between the tissue layers is the smallest amongst all the investigated interfaces.

3.2. Oblique Incidence

The incident wave may strike the boundary between the tissues making some angles (different from 90°) with it. This represents the case of oblique incidence. Two types of oblique incidence are usually considered depending on whether the electric field is in the plane of incidence (parallel polarization) or normal to it (perpendicular polarization). Both types are discussed in the following subsection.

3.2.1. Parallel Polarization

Fig. 3 illustrates the case of parallel polarization for which the electric field intensity components are in the plane of incidence. The plane of incidence is determined by the axes of the interface and normal to the interface which is the xz-plane for the case indicated in the figure. It can be seen from the figure that the incident, reflected and transmitted electric fields have x and z- components which are $(\vec{E}_{ix}, \vec{E}_{iz})$, $(\vec{E}_{rx}, \vec{E}_{rz})$ and $(\vec{E}_{tx}, \vec{E}_{tz})$, respectively that are in the plane of incidence.

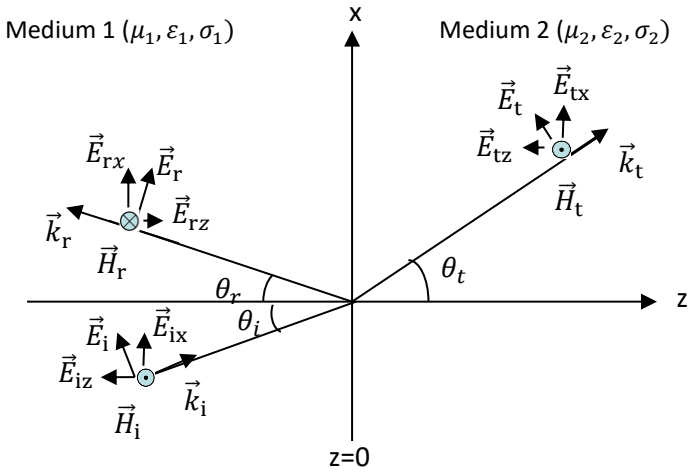

Fig. 3. Oblique incidence/parallel polarization [8]; $\vec{E}_i$, $\vec{E}_r$ and $\vec{E}_t$ are the incident, reflected and transmitted electric field intensities, respectively; $\vec{H}_i$, $\vec{H}_r$ and $\vec{H}_t$ are the incident, reflected and transmitted magnetic field intensities, respectively.

The reflection coefficients for this case ($\Gamma_{||}$) is usually calculated as [8]:

$$\Gamma_{||} = \frac{\eta_2 \cos\theta_t - \eta_1 \cos\theta_i}{\eta_2 \cos\theta_t + \eta_1 \cos\theta_i} \tag{8}$$

where θ_i is the angle of incidence in the first tissue layer and θ_t is the angle of transmission in the second tissue layer.

The angle of transmission can be calculated using Snell's law as:

$$n_1 \sin\theta_i = n_2 \sin\theta_t \quad (9)$$

$$n_1 = c\sqrt{\mu_1 \varepsilon_1} \quad (10)$$

$$n_2 = c\sqrt{\mu_2 \varepsilon_2} \quad (11)$$

where n_1 and n_2 are the refractive indices for the first and second medium, respectively.

The results of the reflection coefficient and loss for this case are summarized in Table 4. They indicate that the reflection coefficient decreases as the angle of incidence increases untill it obtain a zero value at the Brewster's angle θ_B. The Brewster's angle is usually calculated using Eq. (12) [8].

$$\tan\theta_{B_{||}} = \frac{n_2}{n_1} \quad (12)$$

The losses and the reflection loss then increase again for angles larger than the Brewster's angle till they obtain a value of 1 at an angle of 90° at which the wave is incident at the same interface axis. For angles of incidence sufficiently greater than the Brewster angle, the reflection coefficient can be considerably larger than that for the normal incidence such as for the angle 85° at the bone/muscle interface of which the loss is about 183.66% larger than that for normal incidence at the same interface. For the muscle/fat interface, the angles of transmission do not exist at some angles of incidence such as 45° and 75°. This is because substituting these angles in Snell's law with $n_1 > n_2$ results a sine value that is greater than 1 which is not possible.

Table 4. The reflection coefficient $\Gamma_{||}$ and reflection loss for oblique incidence/parallel polarization at 403 MHz.

The interface	n_1	n_2	θ_i	θ_t	$\Gamma_{||}$ $\lvert\Gamma_{||}\rvert \angle \theta_{\Gamma_{||}}{}^o$	The reflection loss [dB]
Bone/muscle	3.62	7.56	10	4.77	$0.38 \angle 171.63$	-8.4
			45	19.79	$0.24 \angle 166.54$	-12.4
			$\theta_B = 64.41$	25.59	≈ 0	No ref
			75	27.55	$0.23 \angle 15.7$	-12.77
			85	28.49	$0.64 \angle 3.35$	-3.88
			90	28.61	1	Total reflection
Muscle/fat	7.56	2.36	10	33.8	$0.48 \angle -5.4$	-6.38
			$\theta_B = 17.34$	72.696	≈ 0	No reflection
			45	-------	-------	------
			75	------	------	------
Fat/skin	2.36	6.84	10	3.43	$0.51 \angle 174.45$	-5.85
			45	14.12	$0.39 \angle 171.7$	-8.18
			$\theta_B = 70.964$	19.04	≈ 0	No ref
			75	19.47	$0.11 \angle 44.54$	-19.17
			85	20.1	$0.56 \angle 4.6$	-5.04
			90	20.184	$1 \angle 0$	Total reflection

3.2.2. Perpendicular Polarization

For this type of oblique incidence, the electric field intensity has a component that is normal to the plane of incidence which is the y-component in this case as depicted in Fig. 4, in which the dot inside the circle indicates that the electric field is out of the plane in the y-axis direction.

The reflection coefficient for this type of oblique incidence (Γ_P) is calculated as:

$$\Gamma_{\perp} = \frac{\eta_2 \cos\theta_i - \eta_1 \cos\theta_t}{\eta_2 \cos\theta_i + \eta_1 \cos\theta_t} \quad (13)$$

The results are summarized in Table 5.

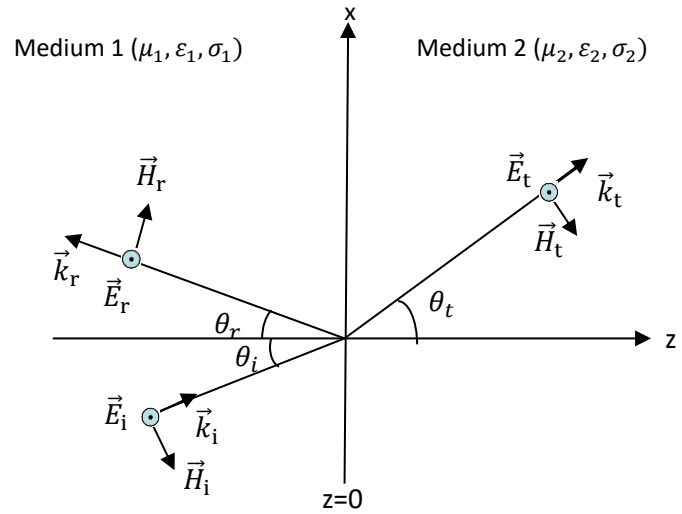

Fig. 4. Oblique incidence/perpendicular polarization [8]; .$\vec{E}_i$, $\vec{E}_r$ and $\vec{E}_t$ are the incident, reflected and transmitted electric field intensities, respectively; $\vec{H}_i$, $\vec{H}_r$ and $\vec{H}_t$ are the incident, reflected and transmitted magnetic field intensities, respectively.

Table 5. The reflection coefficient $\Gamma_\perp$ and the reflection loss for oblique incidence/perpendicular polarization at 403 MHz.

The interface	n_1	n_2	θ_i	θ_t	$\Gamma_\perp$ $\lvert\Gamma_\perp\rvert \angle \theta_\perp{}^o$	The reflection loss [dB]
Bone/muscle	3.62	7.56	10	4.77	$0.39 \angle 171.94$	-8.18
			45	19.79	$0.5 \angle 174.42$	-6.02
			75	27.55	$0.77 \angle 178$	-2.27
			85	28.49	$0.92 \angle 179.35$	-0.72
			90	28.61	$1 \angle 180$	Total reflection
Muscle/fat	7.56	2.36	10	33.8	$0.6 \angle$ -3.61	-4.44
			45	-------	-------	-------
			75	-------	-------	-------
Fat/skin	2.36	6.84	10	3.43	$0.52 \angle 174.62$	-5.68
			45	14.12	$0.62 \angle 176.2$	-4.15
			75	19.47	$0.83 \angle 175.5$	-1.62
			85	20.1	$0.942 \angle 179.55$	-0.52
			90	20.184	$1 \angle 180$	Total reflection

The results in the table indicate that the reflection coefficient increases with angles. Larger reflection coefficient is obtained in this case than that for parallel polarization at the same angle. For example, about 106.64% larger reflection coefficient is obtained at 85º for the case of bone/muscle interface at perpendicular polarization than that for parallel polarization. For the muscle/fat interface, the angles of transmission do not exist at some angles of incidence such as 45º and 75º again for the same reason mentioned in the previous section. The Brewster's angle (θ_{BP}) given in Eq. (14) does not exist in this case because for

nonmagnetic media such as the human body tissues $\mu_1 = \mu_2 = \mu_0$, the $\sin^2\theta_{BP}$ goes to ∞. However, the sine of an angle is never greater than unity [8].

$$\sin^2\theta_{B_\perp} = \frac{1 - \frac{\mu_1\varepsilon_2}{\mu_2\varepsilon_1}}{1 - (\frac{\mu_1}{\mu_2})^2} \quad (14)$$

The reflection coefficient has a value of -1 at 90° which represents the case of total reflection (indicated by total reflection in the table). The reflected wave for this case combines with the incident wave in the medium of incidence to form a standing wave which stands and does not travel.

The reflection coefficient is calculated as ratios in the 6th column of Tables 4 and 5. When the reflection coefficient value is zero, it means that no reflection will happen and the signal will be totally transmitted:

$$P_T = P_{in} - \Gamma^2 P_{in} \quad (15)$$

Where P_T [W] is the power of the signal transmitted from the first medium to the second medium across the interface, P_{in} [W] is the power of the signal incident on the interface and $\Gamma^2 P_{in}$ [W] represents the reflected power. When $\Gamma = 0$, the incident signal will be totally transmitted ($P_T = P_{in}$) and no power will be reflected ($\Gamma^2 P_{in} = 0$), i.e. no reflection losses. However, the reflection loss in dB ($L_r = 20\log_{10}0$) is undefined when $\Gamma = 0$. To indicate the actual case of no reflection losses and that the entire input power of the incident signal is transmitted "No reflection" is indicated in the tables. When $\Gamma = 1$ which occurs at the angle of 90^o, the reflection losses in dB ($L_r = 20\log_{10}1$) will be equal to zero. However, this is not the actual case as the incident signal will be totally reflected for this case and no signal part will be transmitted ($P_T = P_{in} - \Gamma^2 P_{in}$, $P_T = 0$ when $\Gamma = 1$). Therefore, "Total reflection" is indicated in the tables.

The results in the previous sections show that considerable extra reflection losses might be obtained if the wave is incident obliquely at the interfaces between the human body tissue layers. In real scenarios, the angle of incidence is unknown. Hence, the maximum possible loss should be taken into consideration. Based on the results obtained in this paper, this loss can be calculated at a maximum angle below 90^o for the case of perpendicular polarization (85^o for the results in this paper). The extra losses obtained for the case of oblique incidence can be modeled as a link margin which is added to the reflection losses obtained for the case of normal incidence. The link margin represents the difference between the summation of the maximum reflection losses for oblique incidence at all the boundaries and that for normal incidence as:

$$L_r[dB] = L_{r,normal\ incidence} + LM \quad (16)$$

By a way or another, the maximum reflection losses of oblique incidence should be considered.

4. ANALYSIS OF MULTIPLE REFLECTIONS

Multiple reflections are possible in the multilayer human body. The case of multiple reflections for both of normal and oblique incidence is illustrated in Fig. 5.

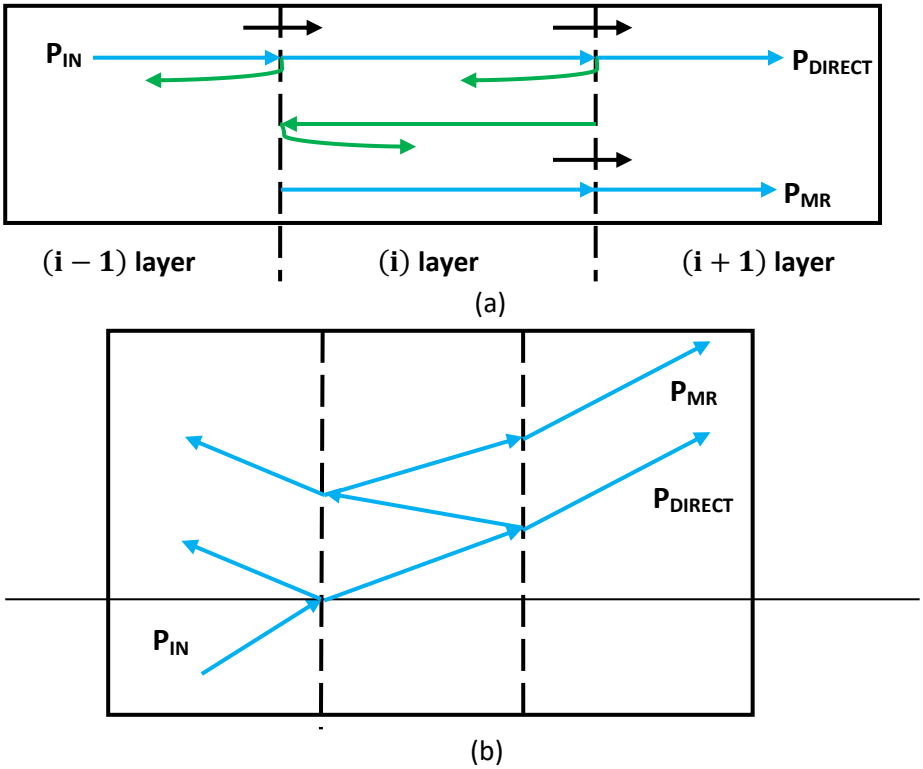

Fig. 5. Multiple reflections path: a) normal incidence [17]; b) oblique incidence.

When the signal passes from one layer to the next one, i.e. from $(i-1)$ layer to (i) layer, part of it is reflected. The remaining signal part transmitted to the next layer ((i) layer) will pass through it and then reflected back at the boundary between this layer and the layer after it (between (i) and $(i+1)$ layers). This reflected part of the signal propagates in the reverse direction in the (i) layer till it arrives the boundary between the (i) and $(i-1)$ layers at which the signal is reflected again. The remaining signal part then continues to propagate in the (i) layer again towards the $(i+1)$ layer. Hence, the signal obtained from multiple reflections (P_{MR}) with the direct signal (P_{DIRECT}) contributes to the total signal transmitted to the $(i+1)$ layer [17]. The difference in the power attenuation of the direct power and multiple reflections signal depends on:

- The reflection between the $(i-1)$ and (i) layers.
- The reflection between the (i) and $(i+1)$ layers.
- Two times the attenuation loss in the (i) layer as the signal passes forward and backward between the $(i-1)$ and $(i+1)$ layers. The attenuation loss L_α [dB] in each tissue layer is calculated as [25]:

$$L_\alpha = 20\log_{10}\left(e^{-\alpha d}\right) \tag{17}$$

where d [m] is the distance the signal travels in the tissue layer and α [Np/m] is the attenuation constant which is calculated as [8]:

$$\alpha = \omega\sqrt{\mu\epsilon}\left[\frac{1}{2}\left(\sqrt{1+\left(\frac{\sigma}{\omega\varepsilon}\right)^2}-1\right)\right]^{1/2} \tag{18}$$

The attenuation constant, at 403 MHz for each tissue layer of the model under investigations, is calculated based on the data in Table 1 and summarized in Table 6.

Table 6. The attenuation constant at 403 MHz for the model's tissue layers.

The tissue layer	α [Np/m]
Bone	4.7
Muscle	19
Fat	3.24
Skin	18.13

The power attenuation difference (L_{diff}) between the multiple reflection signal and direct signal transmitted to the $(i+1)$ layer can be calculated as [17]:

$$L_{diff}(dB) = L_{r(i-1),(i)}(dB) - 2L_{a\,(i)}(dB) + L_{r\,(i),(i+1)}(dB) \quad (19)$$

where $L_{r(i-1),(i)}$ is the reflection loss between the $(i-1)$ and (i) layers, $L_{a\,(i)}$ is the attenuation loss in the (i) layer and $L_{r\,(i),(i+1)}$ is the reflection loss between the (i) and $(i+1)$ layers. L_{diff} is calculated for the bone-muscle-fat layers as an example. The bone, muscle and fat layers are the $(i-1)$, (i) and $(i+1)$ layers, respectively for this case. A thickness of 4 mm is considered for the fat layer. The reflection losses for the case of oblique incidence are calculated at 10^{o}. The calculations for the cases of normal and oblique incidence are summarized in Table 7.

Table 7. The power attenuation difference between the direct and multiple reflection signal at 403 MHz for bone-muscle-fat.

Incidence	$L_{r(i-1),(i)}$ [dB]	$2L_{a\,(i)}$ [dB]	$L_{r\,(i),(i+1)}$ [dB]	L_{diff} [dB]
Normal incidence	-8.4	0.225	-5.19	-13.815
Oblique incidence/parallel polarization	-8.4	0.225	-6.38	-15
Oblique incidence/perpendicular polarization	-8.18	0.225	-4.44	-12.845

As shown in Table 7, the differences of the multiple reflection signal and the signal in the direct path are very small. This means that the multiple reflections signal is much smaller than the direct transmitted signal and thus does not contribute significantly to the total signal. These results are in good agreement with those obtained in [17].

5. CONCLUSIONS

In this paper, the effect of oblique incidence on the reflection losses inside a multilayer human body model has been investigated. The losses have been calculated for the cases of parallel and perpendicular polarization of oblique incidence and compared to that of normal incidence. The results show that larger losses might be obtained for the case of oblique incidence than that for the normal incidence. Hence, it is very important to take the losses of oblique incidence into considerations for accurate overall path loss calculations. The

reflection losses decrease with angles smaller than the Brewster's angle and increase for angles larger than it for the case of parallel polarization. They increase with angles for the case of perpendicular polarization without any correspondence to the Brewster's angle that does not exist for this case considering the nonmagnetic human body tissues. Larger reflection losses are obtained for the case of oblique incidence/perpendicular polarization than that for oblique incidence/parallel polarization at the same angles of incidence. For example 241.16% larger reflection loss is obtained at an incident angle of 85º for the case of oblique incidence/perpendicular polarization at the fat/skin interface in comparison with that for normal incidence. Analysis of the multiple reflections case reveals that the multiple reflections signal is much smaller than the direct transmitted signal for both cases of normal and oblique incidence and thus does not contribute significantly to the total signal.

REFERENCES

[1] A. Ahmed, M. Ur-Rehman, Q. Abbasi, "Miniature implantable antenna design for blood glucose monitoring," *2018 International Applied Computational Electromagnetics Society Symposium*, Denver, CO, pp. 1-2, 2018.

[2] R. Hassan, J. Lee, S. Kim, "A minimally invasive implantable sensor for continuous wireless glucose monitoring based on a passive resonator," *IEEE Antennas and Wireless Propagation Letters*, vol. 19, no. 1, pp. 124-128, 2020.

[3] I. Shah, M. Zada, H. Yoo, "Design and analysis of a compact-sized multiband spiral-shaped implantable antenna for scalp implantable and leadless pacemaker systems," *IEEE Transactions on Antennas and Propagation*, vol. 67, no. 6, pp. 4230-4234, 2019.

[4] R. Alrawashdeh, M. Alhiyari, "The effect of complementary split rings on the performance of on-body patch antenna," *2020 11th International Conference on Information and Communication Systems*, Irbid, Jordan, pp. 425-428, 2020.

[5] A. Damaj, H. El Misilmani, S. Chahine, "Implantable antennas for biomedical applications: an overview on alternative antenna design methods and challenges," *2018 International Conference on High Performance Computing & Simulation*, Orleans, pp. 31-37, 2018.

[6] M. Kod, J. Zhou, Y. Huang, M. Stanley, M. Hussein, A. Sohrab, R. Alrawashdeh, G. Wang, "Feasibility study of using the housing cases of implantable devices as antennas," *IEEE Access*, vol. 4, pp. 6939-6949, 2016.

[7] R. Li, B. Li, G. Du, X. Sun, H. Sun, "A compact broadband antenna with dual-resonance for implantable devices," *Micromachines (Basel),* vol. 10, no. 59 , pp. 1-7, 2019.

[8] M. Sadiku, *Elements of Electromagnetics*, New York: Oxford University Press, 2015.

[9] A. Abdi, H. Aliakbarian, "A miniaturized UHF-band rectenna for power transmission to deep-body implantable devices," *IEEE Journal of Translational Engineering in Health and Medicine*, vol. 7, pp. 1-11, 2019.

[10] A. Kanatas, K. Nikita, P. Mathiopoulos, *New Directions in Wireless Communications Systems: From Mobile to 5G*, Florida: CRC Press Taylor and Francis Group, 2018.

[11] D. Kurup, G. Vermeeren, E. Tanghe, W. Joseph, L. Martens, "In-to-Out body antenna-independent path loss model for multilayered tissues and heterogeneous medium," *Sensors (Basel)*, vol. 15, no. 1, pp. 408–421, 2015.

[12] R. Alrawashdeh, "Path loss estimation for bone implantable applications," *Jordanian Journal of Computers and Information Technology*, vol. 4, no. 02, pp. 94-101, 2018.

[13] G. Vermeeren, E. Tanghe, A. Thielens, L. Martens, W. Joseph, "In-to-out body path loss for wireless radio frequency capsule endoscopy in a human body," *2016 38th Annual International Conference of the IEEE Engineering in Medicine and Biology Society*, Orlando, FL, pp. 3048-3051, 2016.

[14] P. Ara, K. Yu, S. Cheng, E. Dutkiewicz, M. Heimlich, "Human abdomen path-loss modeling and location estimation of wireless capsule endoscope using round-trip propagation loss," *IEEE Sensors Journal*, vol. 18, no. 8, pp. 3266–3277, 2018.

[15] V. Kaim, B. Kanaujia, S. Kumar, H. Choi, K. Kim, K. Rambabu, "Ultra-miniature circularly polarized CPW-fed implantable antenna design and its validation for biotelemetry applications," *Scientific Rep*orts, vol. 10, no. 6795, pp. 1-16, 2020.

[16] M. Haerinia, S. Noghanian, "Analysis of misalignment effects on link budget of an implantable antenna," *2019 URSI International Symposium on Electromagnetic Theory*, San Diego, CA, USA, pp. 1-4, 2019.

[17] I. Dove, *Analysis of Radio Propagation Inside the Human Body for In-Body Localization Purposes*, Department of electrical Engineering, University of Twente, The Netherlands, 2014.

[18] M. Ramezani, V. Blanes-Vidal, E. Nadimi, "An adaptive path loss channel model for wave propagation in multilayer transmission medium," *Progress In Electromagnetics Research*, vol. 150, pp. 1–12, 2015.

[19] D. Kurup, W. Joseph, G. Vermeeren, L. Martens, "In-body path loss model for homogeneous human tissues," *IEEE Transactions on Electromagnetic Compatibility*, vol. 54, no. 3, pp. 556-564, 2012.

[20] P. Zakavi, N. Karmakar, I. Griggs, "Wireless orthopedic pin for bone healing and growth: antenna development," *IEEE Transactions on Antennas and Propagation*, vol. 58, no. 12, pp. 4069-4074, 2010.

[21] M. Bataineh, "Plane wave visualisation on a dielectric-dielectric interface," *The International Journal of Electrical Engineering and Education*, vol. 40, no. 2, pp. 112–122, 2003.

[22] Electromagnetic compatibility and Radio Spectrum Matters; Short Range Devices; Ultra Low Power Active Medical Implants and Peripheralsoperating in the frequency range 402 MHz to 405 MHz; Part 1 and Part 2, *European Telecommunications Standards Institute,* Std. EN 301 839-1/2 V1.3.1, 2007. < www.etsi.org>

[23] Electromagnetic compatibility and Radio Spectrum Matters; Short Range Devices; Ultra Low Power Active Medical Implants and Peripherals operating in the frequency range 401 MHz to 402 MHz and 405 MHz to 406 MHz; Part 1, *European Telecommunications Standards Institute,* Std. EN 302537-1V1.3.1, 2007. < www.etsi.org>

[24] M. Islam, M. Yuce, "Review of medical implant communication system (MICS) band and network," *ICT Express*, vol. 2, no. 4, pp. 188-194, 2016.

[25] R. Alrawashdeh*, Implantable Antennas for Biomedical Applications*, Ph.D dissertation, University of Liverpool, Liverpool, U.K., 2015.

[26] D. Andreuccetti, R. Fossi, C. Petrucci, "Calculation of the dielectric properties of body tissues in the frequency range 10 Hz - 100 GHz," *Institute for Applied Physics*, Italian National Research Council, Florence (Italy), 1997. <http://niremf.ifac.cnr.it/tissprop/>